Journal of Pathology
J Pathol May 2022; **257:** 109–124
Published online 15 February 2022 in Wiley Online Library (wileyonlinelibrary.com) DOI: 10.1002/path.5873

ORIGINAL ARTICLE

Genetic context of oncogenic drivers dictates vascular sarcoma development in *aP2–Cre* mice

Jason A Hanna[1,2,3*], Casey G Langdon[1], Matthew R Garcia[1], Annaleigh Benton[2,3], Nadia A Lanman[3,4], David Finkelstein[5], Jerold E Rehg[6] and Mark E Hatley[1*]

[1] *Department of Oncology, St. Jude Children's Research Hospital, Memphis, TN, USA*
[2] *Department of Biological Sciences, Purdue University, West Lafayette, IN, USA*
[3] *Purdue University Center for Cancer Research, Purdue University, West Lafayette, IN, USA*
[4] *Department of Comparative Pathobiology, Purdue University, West Lafayette, IN, USA*
[5] *Department of Computational Biology, St. Jude Children's Research Hospital, Memphis, TN, USA*
[6] *Department of Pathology, St. Jude Children's Research Hospital, Memphis, TN, USA*

**Correspondence to: ME Hatley, Department of Oncology, St. Jude Children's Research Hospital, 262 Danny Thomas Place, MS-354, Memphis, TN 38105, USA. E-mail: mark.hatley@stjude.org; JA Hanna, Department of Biological Science, Purdue University, 201 S. University Street, West Lafayette, IN 47906, USA. E-mail: hannaja@purdue.edu*

Abstract

Angiosarcomas are aggressive vascular sarcomas that arise from endothelial cells and have an extremely poor prognosis. Because of the rarity of angiosarcomas, knowledge of molecular drivers and optimized treatment strategies is lacking, highlighting the need for *in vivo* models to study the disease. Previously, we generated genetically engineered mouse models of angiosarcoma driven by *aP2–Cre*–mediated biallelic loss of *Dicer1* or conditional activation of $Kras^{G12D}$ with *Cdkn2a* loss that histologically and genetically resemble human tumors. In the present study, we found that DICER1 functions as a potent tumor suppressor and its deletion, in combination with either $KRAS^{G12D}$ expression or *Cdkn2a* loss, is associated with angiosarcoma development. Independent of the genetic driver, the mTOR pathway was activated in all murine angiosarcoma models. Direct activation of the mTOR pathway by conditional deletion of *Tsc1* with *aP2–Cre* resulted in tumors that resemble intermediate grade human kaposiform hemangioendotheliomas, indicating that mTOR activation was not sufficient to drive the malignant angiosarcoma phenotype. Genetic dissection of the spectrum of vascular tumors identified genes specifically regulated in the aggressive murine angiosarcomas that are also enriched in human angiosarcoma. The genetic dissection driving the transition across the malignant spectrum of endothelial sarcomas provides an opportunity to identify key determinants of the malignant phenotype, novel therapies for angiosarcoma, and novel *in vivo* models to further explore angiosarcoma pathogenesis.

Keywords: sarcoma; angiosarcoma; DICER1; kaposiform hemangioendothelioma; TSC1

Received 6 September 2021; Revised 6 January 2022; Accepted 20 January 2022

No conflicts of interest were declared.

Introduction

Normal endothelial cell function is critical for vascular development and cardiovascular health. The abnormal organization and proliferation of endothelial cells can lead to a wide spectrum of vascular malformations and neoplasms, ranging from benign hemangiomas to metastatic angiosarcomas. The classification of each of these neoplasms can be challenging, but is critical for patient care. The International Society for the Study of Vascular Anomalies developed a classification system that is adopted broadly and used clinically [1]. First, vascular anomalies are classified as either vascular malformations or vascular tumors. Vascular tumors are then subclassified based upon malignant potential. Benign vascular tumors include infantile hemangiomas, congenital hemangiomas, tufted angiomas, and others. Vascular tumors of intermediate malignant potential can be locally aggressive but rarely metastasize and include kaposiform hemangioendotheliomas (KHE), Kaposi sarcomas, and others. KHE tumors can be especially difficult to manage, as 70% of KHE patients develop a severe thrombocytopenia from platelet trapping within the tumors known as Kasabach–Merritt phenomenon [2]. Malignant vascular tumors include epithelioid hemangioendothelioma driven by TAZ–CAMTA1 or YAP–TFE3 oncofusion proteins as well as angiosarcoma [3,4].

Patients with angiosarcoma have a poor prognosis, with a 5-year survival of 30–40% [5]. Angiosarcomas can arise in various anatomic locations spontaneously/*de novo* (primary angiosarcoma) or following exposure to toxins, radiation, UV damage, or chronic lymphedema (secondary angiosarcoma). Recent efforts to sequence angiosarcoma tumors and subclassify patients have identified some recurrent mutations and differential patient clusters [6–10]. Such studies have identified recurrent putative driver mutations in genes such as *TP53*, *KDR*, *PIK3CA*, *RAS*, *ARID1A*, *POT1*, *PTPRB*, and *PLCG1*. Similar mutations have been reported recently in studies of canine hemangiosarcomas where *TP53*, *PIK3CA*, *NRAS*, *PTEN*, and *PLCG1* are the most commonly mutated genes [11–14]. These studies have begun to reveal common aberrations among specific anatomic locations and subtypes of tumors. In primary breast angiosarcomas, *PIK3CA* (16–50%) and *RAS* (11–16%) mutations have been observed [8,10]. In addition, *MYC* amplification is reported in many secondary angiosarcomas, whereas *CDKN2A* losses are associated with patients with no radiation exposure or *MYC* amplification [7,15]. Data from the Angiosarcoma Project and others are highly suggestive of effective immunotherapy responses, particularly in head/neck angiosarcoma patients with a high tumor mutation burden [8,10,16]. Despite this greater understanding of the genomic landscape of angiosarcoma, optimal treatment strategies for many patients are still lacking. Furthermore, due to the rarity of vascular tumors, there are few resources for studying the etiology and mechanisms of transformation [17].

We previously generated and characterized novel genetically engineered mouse models (GEMMs) of angiosarcoma [18,19]. In these models, the conditional deletion of *Dicer1* or the combined activation of oncogenic $Kras^{G12D}$ and inactivation of the tumor suppressor *Cdkn2a* in cells expressing *aP2-Cre* led to angiosarcoma development. We sought to utilize these models to further define the mechanisms of transformation. Here we report our findings that DICER1, RAS–MEK–ERK, and mTOR signaling pathways are important for angiosarcoma. However, the activation of the mTOR pathway alone in cells expressing *aP2-Cre* results in vascular tumor development that mimics human KHE tumors.

Materials and methods

Mouse strains and methods

All experiments involving animal studies were reviewed and approved by the Institutional Animal Care and Use Committee at St. Jude Children's Research Hospital.

All mouse strains were generated and described previously including: *aP2-Cre* (*Tg(Fabp4-Cre)1Jmgr*) [20], $Dicer1^{Flox}$ ($Dicer1^{tm1Smr}$) [21], $LSL\text{-}Kras^{G12D}$ ($Kras^{tm4Tyj}$) [22], $Cdkn2a^{Flox}$ ($Cdkn2a^{tm4Rdp}$) [23], $Tsc1^{Flox}$ ($Tsc1^{tm1Djk}$) [24], and *R26-tdTomato* ($Gt(ROSA)26sor^{tm14(CAG\text{-}tdTomato)/Hze}$) [25], as detailed in supplementary material, Table S1. All mice were maintained on a mixed genetic background; thus, littermate controls were used for each study. Primary genetic AT^{cKO} ($aP2\text{-}Cre;Tsc1^{Fl/Fl}$) tumors were transplanted into the flanks of immunocompromised SCID-Beige animals as described previously [18]. Whole blood was collected from AT^{cKO} tumor mice and littermate controls immediately following euthanasia through cardiac puncture with a syringe precoated with 10% EDTA. Complete blood counts were performed in the St. Jude Children's Research Hospital Veterinary Pathology Core using the Forcyte Analyzer following manufacturer's instructions.

Immunoblots, histology, and immunohistochemistry (IHC)

Protein lysates of cells and tissues were prepared in RIPA lysate buffer as previously described [26]. Protein concentrations were determined by the BCA Protein Assay Kit (23225, Pierce, Rockford, IL, USA). Equally loaded lysates were resolved by SDS-PAGE. Blots were probed overnight at 4 °C with primary antibodies detailed in supplementary material, Table S2. Following washing, the membranes were then probed with the species-appropriate secondary antibody. After washing the membranes again, protein expression was visualized using chemiluminescence Luminol reagent (SC-2048, Santa Cruz Biotechnology, Dallas, TX, USA) and film exposure (45-001-508 Amersham Hyperfilm ECL Film, Cytiva, Marlborough, MA, USA). H&E histology and IHC were performed following standard protocols [27]. The antibodies utilized and staining protocol details are provided in supplementary material, Table S3.

Cell lines and allografts

Cells were obtained from the following sources: HMEC-1 (CRL-3243, American Type Culture Collection [ATCC], Manassas, VA, USA), MS1 (ATCC, CRL-2279), SVR (ATCC, CRL-2280), EOMA (M. Roussel, St. Jude Children's Research Hospital), NIH/3T3 (L. Solario, Purdue University), and C2C12 (S. Kuang, Purdue University). The ADC106 cell line was derived from a cutaneous angiosarcoma from an $aP2\text{-}Cre;Dicer^{cKO};Cdkn2a^{cKO};R26^{tdTom/+}$ mouse. The tumor was diced using a razor blade then passed through a 100 μm filter. HMEC-1 cells were maintained in MCDB131 (15100CV Corning, NY, USA) supplemented with 10 ng/ml EGF (23626, R&D Systems, Minneapolis, MN, USA), 1 μg/ml hydrocortisone (0219456901, MP Biomedicals, Irvine, CA, USA), 1× Glutamax (35050, Gibco/Thermo Fisher Scientific, Waltham, MA, USA), and 10% FBS (SH3091003, Hyclone, Logan, UT, USA). The EOMA, MS1, SVR, C2C12, NIH/3T3, and ADC106 cells were maintained in DMEM (SH30243, Hyclone) with 10% FBS (Hyclone), 1× antibiotic-antimycotic penicillin, streptomycin, and amphotericin B (PSA) (A5955, Sigma-Aldrich, St. Louis, MO, USA) and incubated at 37 °C in 5% CO_2. For low adherence conditions, cells were grown on low attachment plates (3471, Corning) in

neurobasal media (12348, Gibco) supplemented with 10 ng/ml EGF, 20 ng/ml FGF (233-FB-025, R&D Systems), 2× B27 supplement (17504-44, Gibco), 2× Glutamax (35050, Gibco), and 1× PSA. Endothelial tube assays were performed by seeding 1.5×10^5 cells (in 300 µl) per well of a 24-well dish previously coated with 250 µl Matrigel matrix (354234, Corning). Cells were then incubated for 4 h at 37 °C. Cells were treated with trametinib (16292, Cayman Chemical, Ann Arbor, MI, USA) or rapamycin (13346, Cayman Chemical) at indicated concentrations or a kill control (20% DMSO) for 72 h. Cell viability was determined using the Cell Titer Glo Assay (G7570, Promega, Madison, WI, USA) measuring luminescence with a BioTek Synergy 2 (BioTek/Agilent, Winooski, VT, USA). The percentage of growth inhibition was calculated using the following formula: (luminescence of treated well – luminescence from kill control)/(luminescence of vehicle treated well – luminescence from kill control) [28].

RNA and gene expression

Total RNA was isolated from tumors of *aP2-Cre;LSL-Kras^{G12D};Cdkn2a$^{Fl/Fl}$* (AKC^{cKO}, $n = 4$) or *aP2-Cre;Tsc1$^{Fl/Fl}$* (AT^{cKO}, $n = 4$) using a bead mill TissueLyser LT (85600, Qiagen, Valencia, CA, USA) and the miRNEasy mini kit (217004, Qiagen) according to manufacturer's instructions. The GeneChip Mouse Gene 2.0 ST Microarray was utilized for gene expression analysis. Gene expression data will be available in NCBI's Gene Expression Omnibus (GEO accession GSE191239). Signal data were summarized by the RMA method, Z-score batch corrected, and compared statistically by unequal variance *t*-tests for each probe set (Partek Genomics Suite 6.6, St. Louis, MO, USA). Then, a Benjamini–Hochberg multiple test correction was applied to limit the false discovery rate (FDR) [29]. We utilized the previously described cohort GSE85834 of *aP2-Cre;Dicer1^{cKO}* tumors, normal aorta, and normal quadriceps for comparisons [18]. Two human angiosarcoma cohorts previously described were also used for comparison [9,30] and a statistical analysis performed with DESeq2 v.1.26.0 [31]. Mouse and human gene orthologs were identified using the BiomaRt Bioconductor package. The top 508 genes commonly enriched in the human datasets with mouse homologs were used as a gene set for Gene Set Enrichment Analysis (GSEA) [32,33]. Differentially expressed genes were analyzed by gene ontology using the Database for Annotation, Visualization and Integrated Discovery (DAVID) [34]. Functional classification and clustering of terms or pathways were performed based on biological process gene ontology terms (BP_FAT) or Kyoto Encyclopedia of Genes and Genomes (KEGG) pathways [35] with the exclusion of redundant terms.

Reverse phase protein arrays (RPPA)

Lysates were prepared from frozen tumor tissue ($n = 3$) or normal aorta ($n = 3$) in lysis buffer (1% Triton X-100, 50 mM HEPES, pH 7.4, 150 mM NaCl, 1.5 mM $MgCl_2$, 1 mM EGTA, 100 mM NaF, 10 mM Na pyrophosphate, 1 mM Na_3VO_4, 10% glycerol, containing protease inhibitor and phosphatase inhibitors (05056489001 and 04906837001, Roche Applied Science, Indianapolis, IN, USA) with 40 mg tissue/ml lysis buffer. The tissue was homogenized by an electric hand homogenizer, then centrifuged at 4 °C, 14,000 × *g* for 10 min. The concentration of the lysate was determined using a BCA Protein Assay Kit (23225, Pierce) and adjusted to 1.5 µg/µl prior to adding 4× SDS sample buffer (40% glycerol, 8% SDS, 0.25 M Tris–HCl, pH 7.8) and boiling for 5 min. Lysates were then shipped to and analyzed at the RPPA Core Facility at the MD Anderson Cancer Center. Comparisons between normal aorta and AT^{cKO} tumors were made using the normalized linear expression and Student's *t*-test, with a Welch correction for unequal variance and Benjamini–Hochberg adjusted *P* values.

Statistics

Statistical analyses were performed using Prism Version 9 (Graph Pad Software, Inc., San Diego, CA, USA). All results are expressed as the mean ± SEM unless stated otherwise. Pairwise comparisons were performed with a two-tailed, unpaired Student's *t*-test after ensuring normality using the Shapiro–Wilk test. Analyses of data with multiple comparisons were performed with one- or two-way ANOVA, followed by Tukey's multiple comparison tests. A Kaplan–Meier survival analysis was performed using a Log-rank (Mantel–Cox) test. All *P* values <0.05 were considered significant.

Results

Disparate angiosarcoma mouse models converge on RAS–MEK–ERK and mTOR pathway activation

We and others have illustrated that the adipose protein 2 (*aP2*) promoter drives expression of Cre recombinase in endothelial cells in *aP2-Cre* transgenic mice [19,36,37]. Previously, we found that *aP2-Cre;Dicer1$^{Fl/Fl}$* (AD^{cKO}) and *aP2-Cre;LSL-Kras^{G12D};Cdkn2a$^{Fl/Fl}$* (AKC^{cKO}) compound mutant mice spontaneously developed angiosarcomas with epithelioid histology and 100% penetrance [18,19]. These models displayed a marked difference in tumor-free survival, with AD^{cKO} animals developing tumors in 250 days and AKC^{cKO} animals developing tumors in 20 days. Despite the striking difference in genetic drivers, both tumor models displayed similar pathway activity with enhanced phosphorylation of ERK and S6 illustrating activation of the RAS–MEK–ERK and mTOR pathways (see supplementary material, Figure S1A–D). In addition, the AKC^{cKO} tumors lacked enhanced phosphorylated AKT as previously observed in AD^{cKO} tumors [18]. This suggests that *Dicer1* loss- and oncogenic *Kras*-driven tumors ultimately lead to similar downstream signaling consequences.

We sought to determine if gene expression of AKC^{cKO} and AD^{cKO} tumors were similar to gene expression alterations in human angiosarcoma using two recently published human cohorts consisting of 25 total patients [9,30]. We observed 613 commonly enriched genes between the two human cohorts (Figure 1A) and 538 genes commonly increased in AKC^{cKO} and AD^{cKO} tumors, with a fold-change >2 and FDR < 0.05. Overlap analysis of these gene sets revealed a significant enrichment of 123 genes increased in expression in both mouse and human angiosarcoma (Figure 1B). GSEA [32,33] indicated that the mouse angiosarcoma upregulated genes were also significantly enriched in human angiosarcomas (Figure 1C). Finally, gene ontology analysis of the 123 overlapping genes revealed terms related to cell cycle, extracellular matrix, and blood vessel development (Figure 1D and supplementary material, Table S4) consistent with recent findings in human and canine tumors emphasizing the role of extracellular matrix [12,38]. Furthermore, pathway analysis of genes enriched in the AKC^{cKO} and AD^{cKO} tumors revealed KEGG pathways such as RAP1 signaling, pathways in cancer, axon guidance, MAPK signaling, and focal adhesion (see supplementary material, Table S4). Interestingly, these are also enriched pathways In both canine hemangiosarcoma and human angiosarcomas [39].

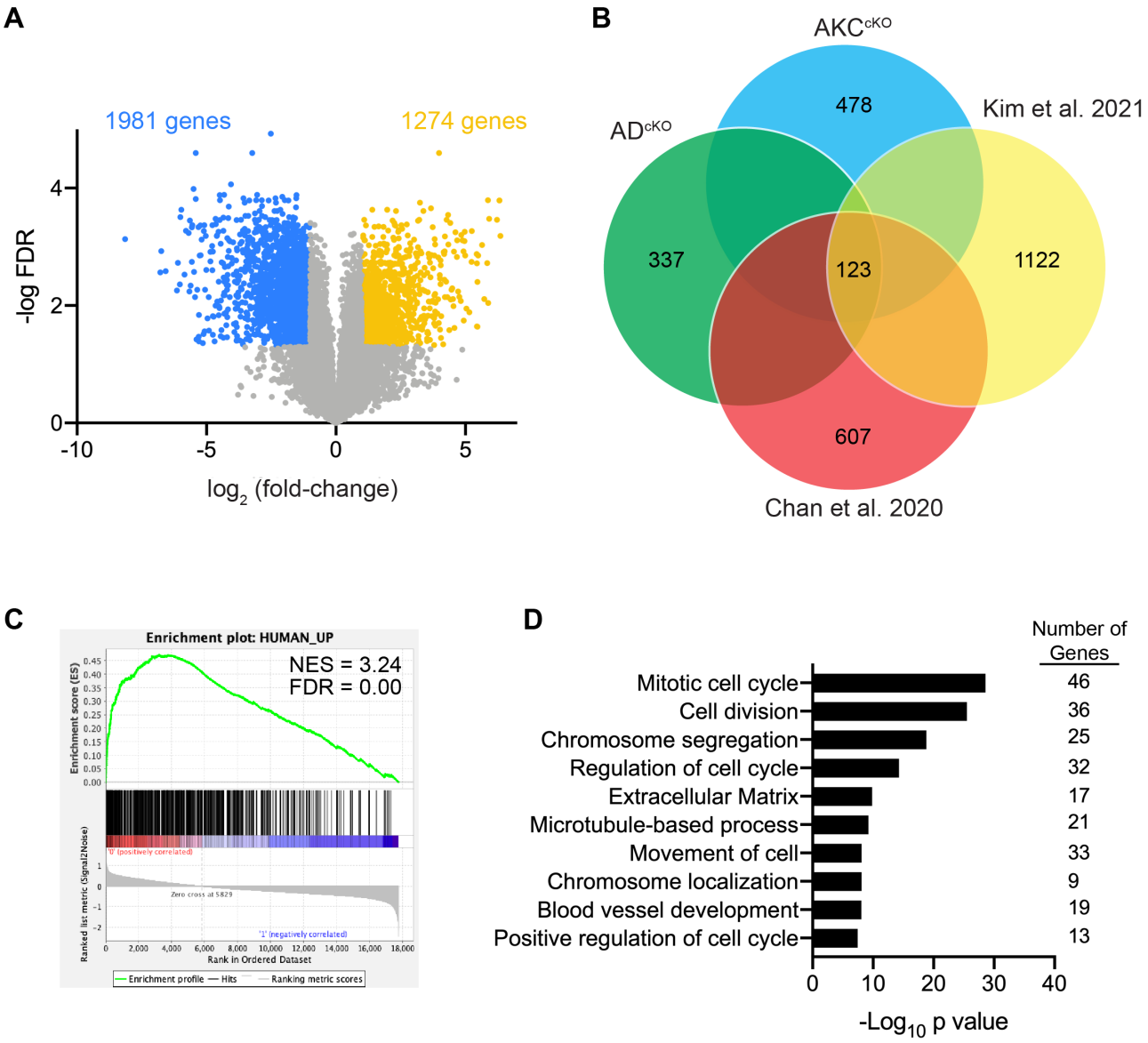

Figure 1. Gene expression alterations in mouse and human angiosarcomas. (A) Volcano plot of the $-\log_{10}$ of the FDR value versus the log fold-change in mRNA expression in AKC^{cKO} angiosarcomas ($n = 4$) versus normal wildtype aortas ($n = 4$) with enriched (yellow) and underrepresented (blue) with FDR < 0.05 and $\log_2$ fold-change >1 or <−1, respectively. (B) Venn diagram of genes increased in expression with FDR < 0.05 and fold-change >2 in AD^{cKO} and AKC^{cKO} (mouse angiosarcomas compared with normal aorta) and human angiosarcomas samples from previously published cohorts [9,30]. (C) GSEA of the genes increased in expression in mouse angiosarcomas compared with the enriched human angiosarcoma gene set with a normalized enrichment score (NES) = 3.24 and FDR = 0.00. (D) Gene ontology enrichment analysis with significantly enriched biological processes (BP_FAT) in the 123 commonly enriched genes in mouse and human angiosarcomas.

$Kras^{G12D}$ and *Cdkn2a* loss cooperate with *Dicer1* deletion

We next sought to determine if $Kras^{G12D}$ or *Cdkn2a* deletion could cooperate with *Dicer1* loss to accelerate tumorigenesis in the AD^{cKO} model. We first generated compound mutant *aP2-Cre;LSL-*$Kras^{G12D}$*;*$Dicer1^{Fl/Fl}$ (AKD^{cKO}) mice to determine the consequences of oncogenic *Kras* activation combined with *Dicer1* loss (see supplementary material, Figure S2A). AKD^{cKO} mice developed tumors with a median onset of 24.5 days (Figure 2A) similar to the time frame of tumor development in *aP2-Cre;LSL-*$Kras^{G12D}$*;*$Cdkn2a^{Fl/Fl}$ (AKC^{cKO}) mice [19]. AKD^{cKO} mice developed tumors predominantly in the interscapular region of the back and in the inguinal adipose, skeletal muscle, abdominal visceral adipose, heart, and lungs. Tumors arose as violaceous, hemorrhagic multicentric masses with areas of necrosis and invasive endothelial cells configured in irregular vascular channels. Cytologic analysis revealed high-grade, large, atypical nuclei and prominent nucleoli analogous to human epithelioid angiosarcomas. These cytologic features are consistent with human angiosarcoma and tumors expressed diagnostic markers of angiosarcomas, including PECAM1, ERG, and PLVAP (Figure 2B and supplementary material, Figure S2B).

In contrast to AKC^{cKO} animals that develop rare cases of other tumors, including malignant triton tumor and pleomorphic spindle cell carcinoma, AKD^{cKO} mice only develop angiosarcomas [19]. AKD^{cKO} animals develop angiosarcoma with similar kinetics to AKC^{cKO} animals, suggesting *Dicer1* loss in this context exhibits equivalent tumor suppressor potency as *Cdkn2a* loss. We previously reported that *aP2-Cre;LSL-*$Kras^{G12D}$ compound mutant mice do not form tumors [19]. Interestingly, *aP2-Cre;LSL-*$Kras^{G12D}$*;*$Dicer^{Fl/+}$ (AKD^{cHet}) animals also developed fully penetrant angiosarcoma with heterozygous deletion of *Dicer1*, suggesting that in this context DICER1 functions as a conventional tumor suppressor where loss of both alleles promotes tumor development (Figure 2A). This contrasts with some mouse models of *Dicer1* deletion where it functions as a haploinsufficient tumor suppressor [40,41].

Given that tumors in AKD^{cKO} and AKC^{cKO} mice display the same kinetics and histology, we next wanted to determine if *Cdkn2a* loss and *Dicer1* loss performed redundant roles in angiosarcoma development. To determine this, we next asked if *Cdkn2a* deletion accelerated tumor onset for the AD^{cKO} model. For this, we bred *aP2-Cre;*$Dicer1^{Fl/+}$*;*$Cdkn2a^{Fl/+}$ ($AD^{cHet}C^{cHet}$) mice to $Cdkn2a^{Fl/+}$*;*$Dicer1^{Fl/+}$ mice and compared tumor development in *aP2-Cre;*$Cdkn2a^{Fl/Fl}$ (AC^{cKO}), *aP2-Cre;*$Dicer1^{Fl/Fl}$ (AD^{cKO}) *aP2-Cre;*$Cdkn2a^{Fl/Fl}$*;*$Dicer1^{Fl/Fl}$ ($AD^{cKO}C^{cKO}$) littermates (see supplementary material, Figure S2C). Indeed, $AD^{cKO}C^{cKO}$ mice developed tumors with a median onset of 125 days compared with 243 days in AD^{cKO} mice (Figure 2C). Angiosarcomas also developed in *aP2-Cre;*$Dicer1^{Fl/Fl}Cdkn2a^{Fl/+}$ ($AD^{cKO}C^{cHet}$) (Figure 2D) with 100% penetrance. Again, angiosarcomas primarily developed in the interscapular region of the back and anatomic locations, as in AD^{cKO} and AKC^{cKO} mice. The angiosarcoma tumors that developed appeared to be histologically similar to AD^{cKO} tumors and expressed diagnostic markers of angiosarcomas, including PECAM1, CD34, ERG, and PLVAP (Figure 2E and supplementary material, Figure S2D).

We previously reported no observable tumor development in *aP2-Cre;*$Cdkn2a^{cKO}$ (AC^{cKO}) mice up to 200 days [42]. We have now extended our observation of AC^{cKO} animals to over 600 days and found that they developed histiocytic sarcomas with 87.5% penetrance and a median tumor-free survival of 350 days (Figure 2C,D). Histiocytic sarcomas are thought to arise from non-Langerhans histiocytic cells of the monocyte/macrophage lineage [43]. Tumors in AC^{cKO} mice were evident in the livers, spleens, lymph nodes, and the lungs. In the liver, the proliferation of atypical monocytic/macrophages was associated with an extensive granulocyte proliferation that caused effacement, destruction, and necrosis of the hepatic architecture. In the spleen, the granulocytic cell hyperplasia caused follicular atrophy involving the white and red pulp and a marked decrease of T and B cells. The neoplastic cells consisted of pleomorphic and anaplastic cells with atypical mitosis and expressed IBA-1, MHCII, and F4/80 consistent with histiocytic sarcomas (Figure 2F and supplementary material, Figure S2F). Histiocytic sarcomas developed in $AD^{cHet}C^{cKO}$ animals and to a lesser extent in $AD^{cHet}C^{cHet}$ (Figure 2D). Histiocytic sarcoma was never observed in $AD^{cKO}C^{cKO}$ animals, probably because they succumb to high angiosarcoma tumor burden before developing histiocytic sarcoma. Although initially thought to be an adipose-specific protein, aP2 (also known as FABP4) is also expressed in other cell types, including macrophages [36,44]. In the AC^{cKO} animals, histiocytic sarcomas probably developed from aP2-Cre expression in macrophages leading to *Cdkn2a* deletion and transformation.

In comparing the tumor histology and onset kinetics of AKC^{cKO}, AKD^{cKO}, $AD^{cKO}C^{cKO}$, AC^{cKO}, and AD^{cKO} it suggests that *Dicer1* and *Cdkn2a* are not completely functionally redundant tumor suppressors in angiosarcoma. In the context of oncogenic KRAS, the deletion of *Dicer1* or *Cdkn2a* results in rapid tumor development. However, independently only *Dicer1* deletion leads to angiosarcoma development in aP2-Cre-expressing cells, suggesting *Dicer1* ablation provides an oncogenic signal capable of activating both the RAS–MEK–ERK and mTOR pathways, leading to tumorigenesis.

mTOR signaling dependence in murine ADC^{cKO} angiosarcoma

We and others have had difficulty generating cell lines from angiosarcoma tumors [18,45]. We thought that in addition to *Dicer1* deletion, the deletion of *Cdkn2a* may allow angiosarcoma cells to overcome cellular senescence and facilitate angiosarcoma cell line generation. Thus, we isolated tumor cells from an *aP2-Cre;*

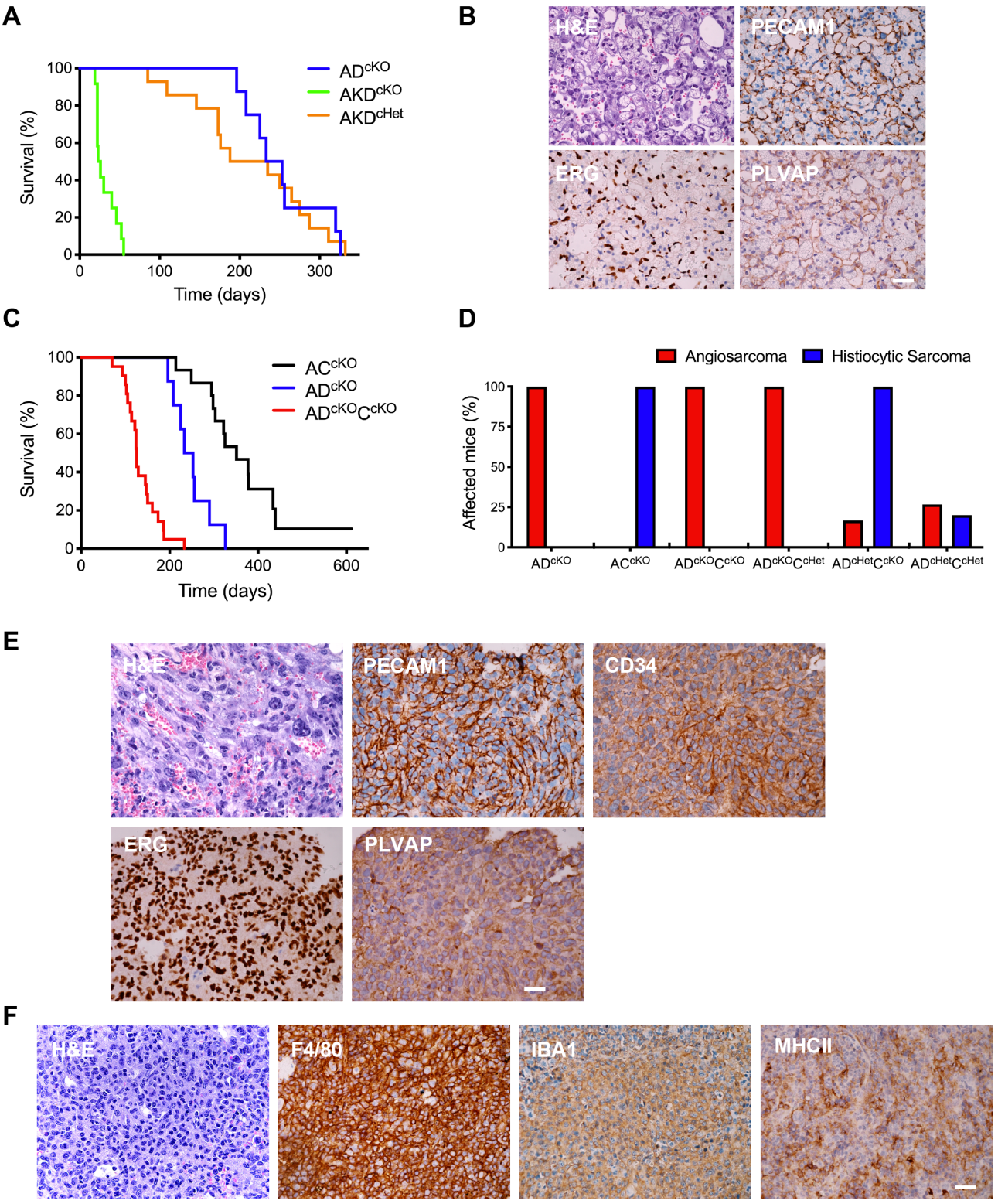

Figure 2. KRAS activation and *Cdkn2a* deletion cooperate with *Dicer1* loss to accelerate angiosarcoma development. (A) Kaplan–Meier survival analysis for *aP2-Cre;Dicer1*$^{Fl/Fl}$ (AD^{cKO}) (blue, $n = 7$), *aP2-Cre;LSL-Kras*^{G12D}*;Dicer1*$^{Fl/Fl}$ (AKD^{cKO})(green, $n = 12$), and *aP2-Cre;LSL-Kras*^{G12D}*;Dicer1*$^{Fl/+}$ (AKD^{cHet})(orange, $n = 14$) Log-rank $p < 0.0001$. (B) Representative histology and IHC staining of an AKD^{cKO} tumor for markers of angiosarcoma, scale bar 25 μm. (C) Kaplan–Meier survival analysis for *aP2-Cre;Cdkn2a*$^{Fl/Fl}$ (AC^{cKO})(black, $n = 16$), *aP2-Cre;Dicer1*$^{Fl/Fl}$ (AD^{cKO}) (blue, $n = 7$), and *aP2-Cre;Dicer1*$^{Fl/Fl}$*;Cdkn2a*$^{Fl/Fl}$ (AD^{cKO}C^{cKO}) (red, $n = 21$). Log-rank $p < 0.0001$. (D) Histogram of tumor types that developed in the indicated genotype. (E) Representative histology and IHC staining for markers of angiosarcoma from an *aP2-Cre;Dicer1*$^{F/Fl}$*;Cdkn2a*$^{Fl/Fl}$ (AD^{cKO}C^{cKO}) tumor, scale bar 25 μm. (F) Representative histology and IHC staining for markers of histiocytic sarcomas from an *aP2-Cre;Cdkn2a*$^{Fl/Fl}$ (AC^{cKO}) tumor, scale bar 25 μm.

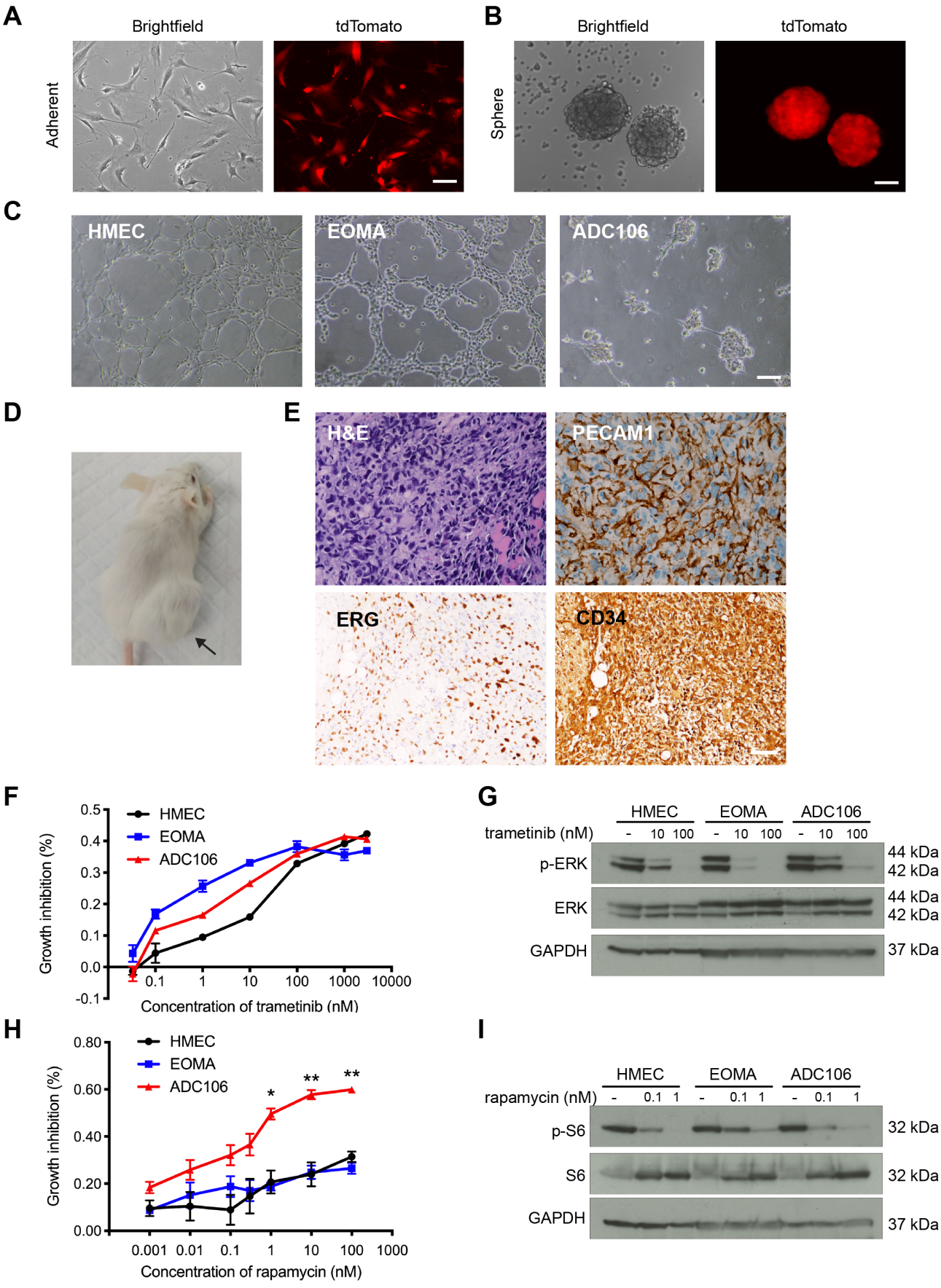

Figure 3 Legend on next page.

Dicer$^{Fl/Fl}$;*Cdkn2a*$^{Fl/Fl}$;*R26*$^{Tom/+}$ (AD^{cKO}C^{cKO}T) mouse where the tumor cells express the tdTomato fluorescent reporter indicating Cre recombinase activity in the tumor cells [25]. The cells were passaged until a homogenously tdTomato-positive cell line was established (eight passages). We found that this ADC106 cell line was able to grow both in adherent and non-adherent tumor sphere conditions on low attachment plates (Figure 3A,B). We also found that the cells maintained high expression of endothelial genes, such as *Pecam1*, *Erg*, *Kdr*, and *Flt4* (see supplementary material, Figure S3A). We next tested if the ADC106 cells would form endothelial-like tubes when grown on Matrigel, as observed in the human dermal microvascular endothelial HMEC-1 cell lines and the mouse hemangioendothelioma, EOMA cell lines. Unlike the HMEC-1 and EOMA cell lines, the ADC106 cells failed to form organized tubes but instead maintained spheroid growth with disorganized extensions and networks potentially due to their transformed state (Figure 3C). When injected subcutaneously into SCID-Beige immunocompromised mice, ADC106 cells formed tumor allografts that retained histologic characteristics of angiosarcoma and maintained expression of the endothelial cell markers, PECAM1, ERG, and CD34 (Figure 3D,E and supplementary material, Figure S3B). Thus, the ADC106 cells represent a valuable murine angiosarcoma cell line to interrogate angiosarcoma pathobiology *in vitro*.

We and others have previously identified activation of the RAS–MEK–ERK and mTOR pathways in mouse angiosarcoma tumors illustrated by hyperphosphorylation of ERK and S6, respectively (see supplementary material, Figure S1A) [18,46]. To determine the relevance of these pathways in the ADC106 cells, we treated cells with the MEK inhibitor trametinib to inhibit the RAS–MEK–ERK pathway and the mTOR pathway inhibitor rapamycin. ADC106 cells were sensitive to trametinib at similar doses as the HMEC-1 and EOMA cells, with EC_{50} values of 6.3 nM, 19.14 nM, and 3.5 nM, respectively. We observed similar reductions in phospo-ERK expression with trametinib treatment (Figure 3F,G). In contrast, ADC106 cells were significantly more sensitive to rapamycin than the EOMA and HMEC-1 cells, despite similar reductions in phosphorylated S6 levels upon mTOR inhibition with 1 nM rapamycin treatment (Figure 3H,I). Based on this result and this higher dependence of the ADC106 cells on mTOR signaling, we sought to determine the genetic role of the mTOR pathway in angiosarcoma *in vivo*.

Tsc1 deletion cooperates with *Dicer1* loss-driven angiosarcoma

To determine the contribution of the mTOR pathway to angiosarcoma pathogenesis, we conditionally deleted *Hamartin* (*Tsc1*) in our AD^{cKO} angiosarcoma model using *Tsc1*^{Flox} mice [47]. TSC1 negatively regulates the mTOR pathway by functioning in a complex that acts as a GTPase-activating protein of the GTPase RHEB, which activates mTORC1 [48]. We bred *aP2-Cre;Dicer1*$^{Fl/+}$;*Tsc1*$^{Fl/+}$ (AD^{cHet}T^{cHet}) mice to *Dicer1*$^{Fl/+}$;*Tsc1*$^{Fl/+}$ (D^{cHet}T^{cHet}) mice and compared tumor development in littermate offspring (Figure 4A and supplementary material, Figure S4A). *Tsc1* deletion in *aP2-Cre;Dicer1*$^{Fl/Fl}$;*Tsc1*$^{Fl/Fl}$ (AD^{cKO}T^{cKO}) animals accelerated tumor onset without changing the distribution of anatomic location or histologic characteristics of the angiosarcoma tumors found in *aP2-Cre;Dicer1*$^{Fl/Fl}$ (AD^{cKO}) and *aP2-Cre;Dicer1*$^{Fl/Fl}$;*Tsc1*$^{Fl/+}$ (AD^{cKO}T^{cHet}) mice (Figure 4B and supplementary material, Figure S4B). Similar tumors developed in AD^{cKO}T^{cHet} mice, whereas no tumors developed in AD^{cHet}T^{cHet} mice. Thus, mTOR pathway activation cooperates with *Dicer1* deletion to accelerate tumor development. However, tumor onset kinetics suggest that the mTOR pathway and *Cdkn2a* deletion contribute similarly, whereas KRAS^{G12D} oncogene activation dramatically enhances tumor development, suggesting the RAS–MEK–ERK pathway as a major driver in angiosarcoma.

aP2-Cre;Tsc1^{cKO} tumors resemble human KHE

Although *Tsc1* loss contributed to angiosarcoma development in the *Dicer1*^{cKO} model, we also observed tumor development independent of *Dicer1* deletion in aP2-Cre; *Tsc1*$^{Flox/Flox}$ (AT^{cKO}) mice. Therefore, we generated an independent cohort of these mice (see supplementary material, Figure S5A). Interestingly, AT^{cKO} mice developed tumors in their paws (Figure 5A). These paw tumors only developed in animals with homozygous *Tsc1*^{Flox} deletion, but were not observed in the *aP2-Cre;Dicer1*^{cKO};*Tsc1*^{cKO} mice, suggesting *Dicer1* expression is required for the development of these tumors. Because of this interesting anatomic location and similarity to other *Tsc1* tumor models [48–50], we decided to further study these tumors. AT^{cKO} mice developed bilateral hindlimb paw tumors with a median onset of 150 days with 100% penetrance (Figure 5B). Tumors occasionally developed in the forepaw and in

Figure 3. Generation of a novel murine angiosarcoma cell line and activated pathway inhibition. (A) Brightfield and tdTomato fluorescence of ADC106 cells grown in adherent conditions, scale bar 25 μm. (B) Brightfield and tdTomato fluorescence of ADC106 spheres grown in low adherence conditions, scale bar 100 μm. (C) Tube formation assay of HMEC-1, EOMA, and ADC106 cells grown on Matrigel for 4 h, scale bar 25 μm. (D) ADC106 cell allograft formation in SCID-Beige mice, with 1×10^6 cells injected subcutaneously in the flank (arrow). (E) Representative histology and PECAM1, ERG, and CD34 IHC staining of ADC106 cell allograft, scale bar 25 μm. (F) Growth inhibition curve of HMEC-1 (EC_{50} = 19.14 nM), EOMA (EC_{50} = 3.5 nM), and ADC106 (EC_{50} = 6.3 nM) cells treated with the indicated concentration of trametinib, data presented as mean ± SEM. (G) Immunoblot analysis of cells treated with the indicated concentration of trametinib and antibodies probed indicated on the left. (H) Growth inhibition curve of HMEC-1, EOMA, and ADC106 (EC_{50} = 0.96 nM) cells treated with rapamycin, data presented as mean ± SEM (*$p < 0.05$, **$p < 0.01$). (I) Immunoblot analysis of cells treated with rapamycin and antibodies probed indicated on the left.

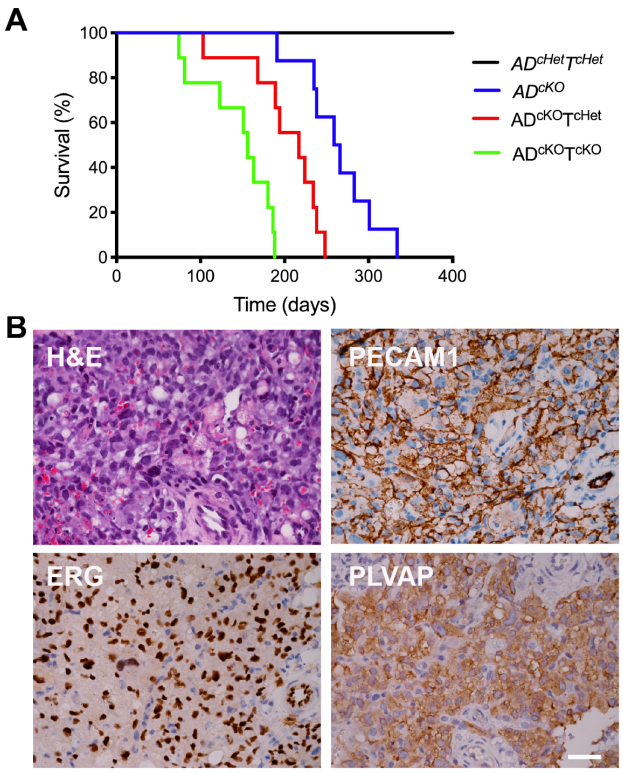

Figure 4. *Tsc1* deletion cooperates with *Dicer1* loss accelerating tumor development. (A) Kaplan–Meier survival analysis of *aP2-Cre;Dicer1*$^{Fl/+}$*;Tsc1*$^{Fl/+}$ (AD^{cHet}T^{cHet})(black, $n = 21$), *aP2-Cre;Dicer1*$^{Fl/Fl}$ (AD^{cKO})(blue, $n = 8$), *aP2-Cre;Dicer1*$^{Fl/Fl}$*;Tsc1*$^{Fl/Fl}$ (AD^{cKO}T^{cKO})(green, $n = 12$), and *aP2-Cre;Tsc1*$^{Fl/Fl}$ (AT^{cKO}) (red, $n = 10$) Log-rank $p < 0.0001$. (B) Representative histology and IHC staining for markers of angiosarcoma in an *aP2-Cre;Dicer1*$^{Fl/Fl}$*;Tsc1*$^{Fl/Fl}$ (AD^{cKO}T^{cKO}) tumor, scale bar 25 μm.

other anatomic locations, including hindlimb muscle, tail, semitendinosus muscle near the tail base, inguinal adipose, and liver (Figure 5C). In addition to the unique anatomic location, these tumors were also histologically distinct from the angiosarcoma tumors described previously in AD^{cKO}, AKC^{cKO}, and ADT^{cKO} animals. Tumors displayed a nodular spindle cell-like morphology with glomeruloid nests reminiscent of Kaposi sarcomas (Figure 5D,E and supplementary material, Figure S5B,C). The tumors expressed markers of endothelial cells, such as PECAM1, CD34, and ERG. They also expressed lymphatic endothelial cell markers, such as FLT4 (VEGFR3) and PROX1 (Figure 5E,F). In contrast, AD^{cKO} and AKC^{cKO} angiosarcomas did not express PROX1 (Figure 5F), suggesting the AT^{cKO} tumors may be derived from lymphatic endothelial cells, in which aP2 is known to be expressed [51].

These features of the AT^{cKO} tumors resembled human KHE. KHE tumors are rare vascular tumors that occur most often in the extremities of infants and exhibit lymphatic endothelial cell differentiation [2]. This anatomic predilection for the extremities is of note given the occurrence of tumor development in the hind paws of the animals. The mouse KHE-like lesions were composed of irregular lobules with coalescing and non-coalescing nodules of spindled cells without nuclear pleomorphism forming elongated slit like lumina or curving around and/or merging with glomeruloid-like areas of round cells. The KHE-like nodules with glomeruloid areas had an alternating positive and negative podoplanin (PDPN) pattern and diffusely positive expression of PECAM1 and CD34 (see supplementary material, Figure S5D). The tumors also had capillary-like areas and some lobulated nodules in the dermis had an occasional large, dilated lymphatic and a few small lymphatics at their periphery (see supplementary material, Figure S5B–D). A few cells expressing alpha-smooth muscle actin (α-SMA; ACTA2) were evident in occasional glomeruloid structures (see supplementary material, Figure S5E). ITGA2B (CD41) IHC, which labels megakaryocytes and platelets, showed that there was an abundant number of platelets in some of the glomeruloid capillary structures, as occurs with microthrombi commonly found in human KHEs (see supplementary material, Figure S5E).

KHE tumors are generally of intermediate malignancy in that they invade locally but rarely metastasize. We transplanted eight AT^{cKO} tumors, including five paw tumors and three inguinal tumors, into the flanks of SCID-Beige immunocompromised mice. We did not observe any allograft tumor growth, unlike the aggressive growth and lung metastasis previously reported for AD^{cKO} allografts [18]. KHE is often associated with a clinical condition known as Kasabach–Merritt phenomenon, a consumptive coagulopathy and thrombocytopenia as a result of platelet entrapment in the tumor [2]. Importantly, we observed a similar thrombocytopenia in tumor-bearing AT^{cKO} animals with a significant decrease in platelets compared with aged-matched controls (Figure 5G). Importantly, RBC counts in tumor mice were not altered compared with control mice (Figure 5H). These results suggest that the tumors in AT^{cKO} mice resemble human KHE, indicating that this is a potential model to study this rare pediatric vascular neoplasm, as well as the Kasabach–Merritt phenomenon.

Integrative transcriptomic and proteomic analysis of KHE-like tumors in AT^{cKO} mice

In order to gain insight into the mechanism by which *Tsc1* deletion drives KHE-like tumor formation in AT^{cKO} mice, we performed mRNA expression profiling of the paw tumors as well as normal mouse aorta. In AT^{cKO} tumors, there were 2,196 genes with increased and 2,381 genes with decreased expression compared with normal aorta, with log ratio > 1 or <−1 and FDR < 0.05 (Figure 6A). Using gene ontology analysis of the 588 most enriched genes in AT^{cKO} KHE-like tumors compared with aorta with log ratio > 2 and FDR < 0.05, we found enrichment of terms involved in cell migration, angiogenesis, and blood vessel morphogenesis and development (Figure 6B). In addition, genes related to lymph vessel development, including *Prox1*, *Flt4*, *Tbx1*, *Sox18*, *Nfatc1*, and *Efnb2*, were also enriched, thus suggesting a potential lymphatic endothelial origin for the AT^{cKO} tumors (see supplementary material, Table S3).

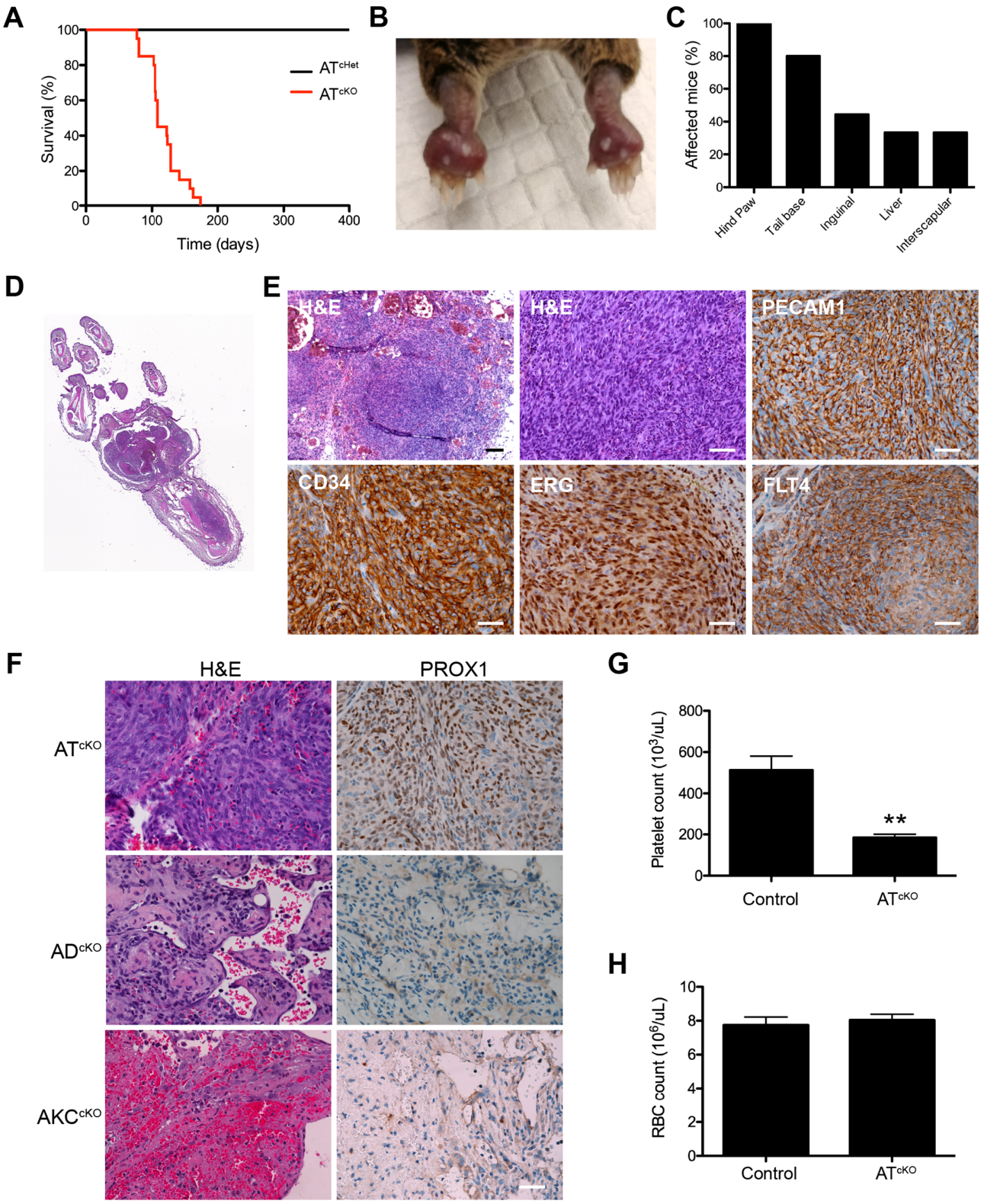

Figure 5. *Tsc1* deletion with *aP2*-Cre results in KHE-like sarcoma tumors in the paw. (A) Kaplan–Meier tumor-free survival analysis in *aP2-Cre;Tsc1*$^{Fl/+}$ (AT^{cHet})(black, $n = 17$) and *aP2-Cre;Tsc1*$^{Fl/Fl}$ (AT^{cKO})(red, $n = 20$), Log-rank $p < 0.0001$. (B) Representative paw tumor in an AT^{cKO} mouse. (C) Histogram of anatomic locations of tumor development in AT^{cKO} mice. (D) Low resolution scan of an H&E-stained paw tumor from an AT^{cKO}. (E) Representative histology and IHC for markers of angiosarcoma (PECAM1, CD34, ERG) and lymphatic endothelial cells (FLT4) in an AT^{cKO} tumor, scale bar 100 μm top left (black), all others 25 μm (white). (F) Representative histology and PROX1 staining of AT^{cKO}, AD^{cKO}, and AKC^{cKO} tumors, scale bar 25 μm. (G) Platelet count (**$p < 0.01$) and (H) RBC count in tumor-bearing AT^{cKO} mice ($n = 4$) and age-matched control animals ($n = 6$), data presented as mean ± SEM.

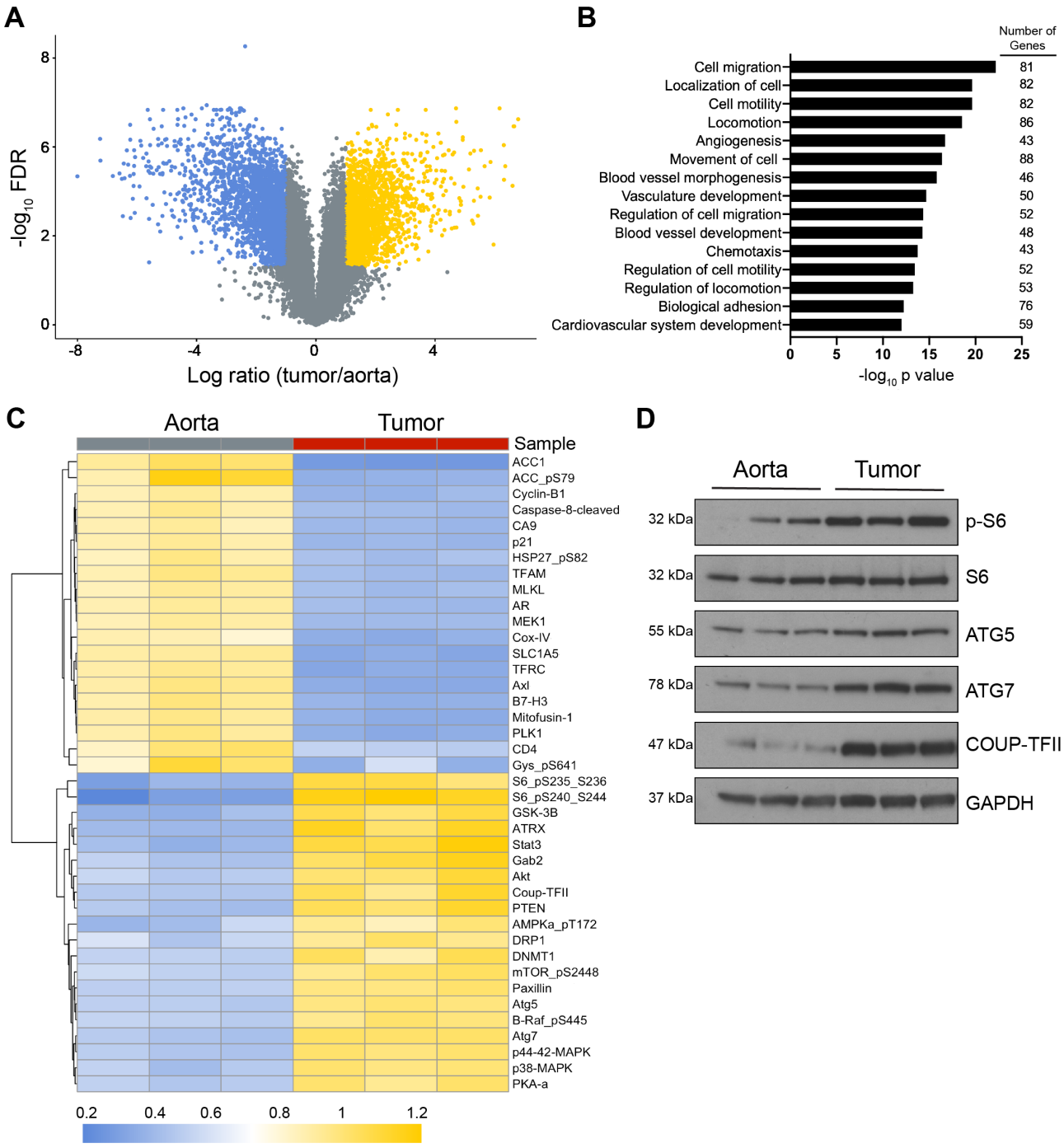

Figure 6. Gene and protein expression in KHE mouse model. (A) Volcano plot of the $-\log_{10}$ of the FDR value versus the log ratio fold-change in mRNA expression in *aP2-Cre;Tsc1*$^{Fl/Fl}$ (AT^{cKO}) ($n = 4$) versus normal aorta ($n = 4$). Genes with FDR < 0.05 and $\log_2$ ratio > 1 (yellow) < −1 (blue). (B) Gene ontology enrichment analysis with significantly enriched biological processes (BP_FAT) in genes upregulated in tissue from AT^{cKO} tumors compared with normal aorta with log ratio > 2 and $p < 0.05$ (588 genes). (C) Heatmap of the top 20 statistically significant up- and downregulated proteins ranked by mean difference in AT^{cKO} tumors ($n = 3$) compared with normal aorta ($n = 3$) by RPPA. Comparisons between normal aorta and AT^{cKO} tumors were made using the normalized linear expression and Student's *t*-test with a Welch correction for unequal variance and Benjamini–Hochberg adjusted *P* values. (D) Immunoblot analysis of lysates from AT^{cKO} tumors and normal aorta. Antibodies used are shown to the right.

To compare the gene expression changes across the GEMMs, we used principal component analysis of transcriptomes, and found that tumors from AD^{cKO}, AKC^{cKO}, and AT^{cKO} mice clustered distinctly (see supplementary material, Figure S6A). However, using the top 8,000 differentially expressed genes of human angiosarcoma, the aggressive AD^{cKO} and AKC^{cKO} tumors clustered together by unsupervised hierarchical clustering, whereas the less aggressive AT^{cKO} tumors clustered more closely with normal aorta and quadricep muscle (see supplementary material, Figure S2B).

To further explore the cell signaling and proteomic consequences in AT^{cKO} tumors compared with normal aorta, we performed RPPA and found the highest differentially expressed protein to be phosphorylated S6 (S240/S244) (Figure 6C and supplementary material, Table S6). Other highly differentially expressed proteins included the COUP-TFII (*NR2F2*) transcription factor known to interact with PROX1, leading to the expression of genes involved in lymphatic endothelial cell differentiation [52]. In addition, the STAT3 transcription factor and DNMT1 DNA methyltransferase were significantly expressed in AT^{cKO} tumors, which were recently shown to be dysregulated in Kaposi's sarcoma, an endothelial cell tumor associated with Kaposi's sarcoma-associated herpesvirus (KSHV, HHV-8) [53].

The autophagy regulators ATG5 and ATG7 were also among the most enriched proteins in the AT^{cKO} tumors, suggesting autophagy to be an important component of these tumors, similar to other *Tsc1*-deleted cells and tumor models [54–56]. To validate some of these expression changes, we performed immunoblot analysis and observed significant enrichment of phosphorylated S6, ATG5, ATG7, and COUP-TFII in AT^{cKO} tumors compared with control aorta lysates (Figure 6D). Thus, AT^{cKO} tumors are a vascular neoplasm resembling less aggressive human lymphatic KHE tumors by histology, gene expression, and cell signaling pathway activation.

Discussion

Pediatric and adult vascular tumors are rare, but can have devastating consequences [57]. Benign tumors can lead to lifelong disfigurement and malignant tumors are difficult to manage clinically, leading to a poor prognosis. Further understanding of the genetic drivers and molecular pathways active in these tumors is key to identifying therapeutic vulnerabilities that benefit these patients [4,58]. The development of GEMMs to model these tumors can provide a valuable resource for studying tumorigenesis *in vivo*. Here we have developed genetically simple, fully penetrant mouse models of angiosarcoma and KHE-like tumors (see supplementary material, Table S7).

MicroRNAs (miRNAs) are short non-coding RNAs that regulate gene expression and are dysregulated in many diseases, including cancer [59,60]. miRNAs are transcribed in the nucleus and undergo a series of processing events. DICER1 is the enzyme that mediates the second cleavage event, resulting in the mature approximately 22 nucleotide long miRNA [61]. A reduction in miRNA processing machinery and a global reduction of miRNAs promote cancer [62,63]. Furthermore, *DICER1* mutations result in a tumor predisposition syndrome where patients inherit an inactivating mutation and often acquire second hit mutations in the RNase IIIb domain, altering miRNA processing and reducing miRNA expression in tumors [64].

In many mouse models of cancer, DICER1 acts as a haploinsufficient tumor suppressor, where loss of one allele promotes tumorigenesis, but loss of both alleles is detrimental to tumor formation and potentially cell survival [40]. Because of this, DICER1 has long been thought to be required for cell survival and there are only a few examples of viable cells with complete *Dicer1* deletion [65,66]. However, we have found that biallelic loss of *Dicer1* in *aP2-Cre* mice is sufficient for angiosarcoma formation independent of any other engineered oncogene or tumor suppressor loss [18]. We hypothesize that the long latency of AD^{cKO} tumors results from the lack of cell viability with complete *Dicer1* loss, the eventual recombination of both $Dicer1^{Flox}$ alleles, survival, and transformation of a *Dicer1*-depleted cell that results in the activation of the RAS–MEK–ERK and mTOR pathways. Alternatively, secondary mutations in AD^{cKO} tumors could lead to downstream pathway activation and tumorigenesis, although this mechanism is challenging due to the 100% penetrance of angiosarcoma development in AD^{cKO} mice.

Furthermore, heterozygous loss of *Dicer1* allows tumor formation when combined with $Kras^{G12D}$, which is accelerated with homozygous deletion, analogous to a conventional tumor suppressor. This suggests that *Dicer1* harbors similar tumor suppressor potency as *Cdkn2a*, which is known to activate both the RB1 and TP53 pathways. The consequences of biallelic *Dicer1* deletion and subsequent loss of miRNAs are still unclear and an ongoing area of investigation. Nonetheless, we found that the loss of *Tsc1* and *Cdkn2a*, or the activation of $Kras^{G12D}$, cooperate with *Dicer1* deletion to drive angiosarcoma development.

DICER1 mutations have been observed in a few angiosarcomas and one recent canine hemangiosarcoma [39]. Specifically, one mutation (Y1091F) was found in a scalp angiosarcoma from a patient with no UV-mutational signature [9]. A truncating mutation (L1191*) has been reported in a recurrence of a radiation-associated tumor [67]. Finally, a patient in the Angiosarcoma Project has been reported to have a non-start (M1L) mutation and a missense (N157T) mutation [8]. A recent study also reported an *AGO2–TRAPPC9* fusion gene in a patient [30]. Mature miRNAs are loaded onto AGO2 to generate the RNA-induced silencing complex for translational repression or mRNA degradation of miRNA target genes [61]. Thus, altered AGO2 could effectively reduce the function of miRNAs. However, the implications of this novel *AGO2–TRAPPC9* fusion gene on AGO2 functions are unclear.

The histiocytic sarcomas in $aP2\text{-}Cre;Cdkn2a^{Fl/Fl}$ (AC^{cKO}) mice highlight that cell type expression of Cre and genetic drivers cooperate to dictate tumorigenesis. Histiocytic sarcoma is thought to arise from macrophage progenitors and as such display morphologic and expression markers of mature histiocytes. Indeed, aP2 has been shown to be expressed in macrophages, where it is involved in inflammation signaling and neutrophil recruitment during infection [68]. Histiocytic sarcomas only developed in animals with *Cdkn2a* deletion,

highlighting its role in histiocytic sarcoma development, which is in agreement with other GEMMs and human histiocytic sarcoma patients [69–71]. However, this highlights the caveat that the potential promiscuity of *aP2-Cre* expression in other cell types introduces the potential for non-cell autonomous contributions in modifying the tumor microenvironments and contributions of other non-endothelial cell types cannot be excluded in these studies.

The combined deletion of *Cdkn2a* and *Dicer1* in *aP2-Cre* animals allowed us to generate a novel murine angiosarcoma cell line, which has been previously challenging for our group and others [18,45]. We validated the endothelial features of the ADC106 cells, found that the cells grow as allografts in immunocompromised mice, and importantly maintain CD31 expression during this process. The ADC106 cells are relatively sensitive to MEK inhibition and mTOR inhibition, providing further evidence for these pathways as attractive targets for combined therapeutic approaches in angiosarcoma [72]. This finding led us to test the genetic contribution of the mTOR pathway in angiosarcoma pathogenesis, which has been shown to be active in human tumors. In fact, mTOR expression was observed in all patients (11/11) by IHC [30]. In other studies, 71–100% of angiosarcoma patients examined exhibited positive expression and increased phosphorylated S6 compared with normal adjacent blood vessels by IHC [49,73]. Furthermore, the mTOR inhibitor everolimus was shown to give the highest progression-free rate in angiosarcoma patients (three patients) compared with other high-grade sarcomas that failed anthracycline and ifosfamide regimens [74].

As anticipated, mTOR pathway activation accelerated angiosarcoma development driven by *Dicer1* loss. Surprisingly, *Tsc1* deletion alone with *aP2-Cre* led to KHE-like tumor development. KHE was first named because of its unmistakable resemblance histologically to Kaposi sarcoma [75]. These rare tumors of infancy most often develop in the extremities and are associated with Kasabach–Merritt phenomenon in over 70% of patients. This thrombocytopenia is thought to arise from platelet trapping in the tumors and leads to fatalities in 10% of patients [2]. We observed a similar reduction in platelets in KHE-like tumor-bearing mice and a similar anatomic location of tumor development with paw and hind limb tumors in the AT^{cKO} mice. Although *TSC1* deletion has not been reported in KHE, exciting results from several groups recently reported efficacious treatment of KHE patients with sirolimus [76,77]. In addition, results should be available soon from a phase 2 clinical trial of sirolimus in vascular anomalies including KHE patients (NCT00975819). The AT^{cKO} model provides a platform for further interrogation of both KHE and the devastating associated Kasabach–Merritt phenomenon.

The anatomic location and expression of lymphatic endothelial cell markers are similar to those of tumors previously reported by Sun and colleagues [49]. In their model, *Tsc1* deletion using *End-Scl-CreERT* leads to vascular tumor development, with nearly 100% penetrance upon tamoxifen administration to adult mice. Cutaneous and liver tumors developed in this model. The cutaneous tumors progressed into lymphangiosarcomas or angiosarcomas of lymphatic origin. Interestingly, *aP2-Cre;*$Tsc1^{cKO}$ (AT^{cKO}) tumors in our study did not progress to aggressive angiosarcomas, as evidence by histologic appearance more resembling intermediately malignant KHE tumors and lack of autonomous allograft tumor growth in immunocompromised mice. This distinction could be a result of differences in the timing of Cre expression (tamoxifen delivery in adults versus *aP2-Cre* during embryogenesis) or expression of Cre recombinase in different subtypes of endothelial cells dictated by differences in *End-Scl-CreERT* and *aP2-Cre* expression. Interestingly, KHE paw tumors were not observed in $AD^{cKO}T^{cKO}$ (*aP2-Cre;*$Dicer1^{Fl/Fl}$;$Tsc1^{Fl/Fl}$) animals, suggesting DICER1 expression is required for these tumors.

Evidence from our model and other models of endothelial and global deletion of *Tsc1* suggests that mTOR pathway activation is insufficient to promote aggressive vascular tumor formation [47,72,78]. Nonetheless, it is apparent that the mTOR pathway is active in vascular tumors. In one study, all 59 angiosarcoma patients examined exhibited increased phosphorylated S6 compared with normal adjacent bloods vessel by IHC [73]. In another study, 71% of patients displayed positive phosphorylated S6 [49].

In summary, we have found that DICER1 can function as a tumor suppressor and cooperate with other genetic drivers of angiosarcoma tumorigenesis. Interrogation of the pathways active in angiosarcoma led us to find that the mTOR pathway alone is insufficient to promote aggressive angiosarcoma, but rather results in KHE-like tumor development. Gene expression analysis across the spectrum of tumor models aligned with human angiosarcoma gene expression analysis suggests that aggressive tumors rely on extracellular matrix modifications to promote cell migration and invasion along with steady proliferation and promotion of inflammatory pathways. These findings provide insights into the pathogenesis of vascular tumors and highlight the key dependencies of specific cell types to transformation. These models can be further interrogated to identify therapeutic vulnerabilities to benefit patients of these clinically challenging vascular tumors.

Acknowledgements

The authors thank Jonathan Graff for *aP2-Cre* mice, Greg Hannon for $Dicer1^{Flox}$ mice, Nabeel Bardeesy and Ronald DePinho for $Cdkn2a^{Flox}$ mice, David Kwiatkowski for $Tsc1^{cKO}$ mice, Martine Roussel for EOMA cells, Shihuan Kuang for C2C12 cells, and Luis Solario for NIH/3T3 cells. We would also like to thank the St. Jude Children's Research Hospital VPC Resource for IHC and histology services and the

Hartwell Center for microarray services. The authors gratefully acknowledge the support of the C^{3}B from the Purdue Center for Cancer Research (NIH grant P30 CA023168), the IU Comprehensive Cancer Center (NIH grant P30 CA082709), the Walther Cancer Foundation, and the Ralph W. and Grace M. Showalter Research Trust (JAH). Research reported in this publication was supported by the National Cancer Institute of the National Institutes of Health under Award Numbers R01CA216344 and R01CA251436 (MEH). The content is solely the responsibility of the authors and does not necessarily represent the official views of the National Institutes of Health. The Hatley laboratory is also supported by grants from The V Foundation for Cancer Research, the Rally Foundation for Childhood Cancer Research and Open Hands Overflowing Hearts award number 20IC23 (MEH), St. Jude Cancer Center Support Grant (P30 CA21765), and American Lebanese Syrian Associated Charities of St. Jude Children's Research Hospital.

Author contributions statement

JH and MH were responsible for study conceptualization and supervision. JH, CL, MG and AB acquired the data. JH, CL, NL, DF, JR and MH were responsible for the analysis, interpretation and visualization of the data. JH drafted the manuscript. All authors were responsible for critical revision of the manuscript.

Data availability statement

The transcriptomic data are deposited in the Gene Expression Omnibus (GEO) under accession number GSE191239 (https://www.ncbi.nlm.nih.gov/geo/query/acc.cgi?acc=GSE191239).

References

1. Dasgupta R, Fishman SJ. ISSVA classification. *Semin Pediatr Surg* 2014; **23:** 158–161.
2. Putra J, Gupta A. Kaposiform haemangioendothelioma: a review with emphasis on histological differential diagnosis. *Pathology* 2017; **49:** 356–362.
3. Tanas MR, Sboner A, Oliveira AM, *et al*. Identification of a disease-defining gene fusion in epithelioid hemangioendothelioma. *Sci Transl Med* 2011; **3:** 98ra82.
4. Florou V, Wilky BA. Current management of angiosarcoma: recent advances and lessons from the past. *Curr Treat Options Oncol* 2021; **22:** 61.
5. Buehler D, Rice SR, Moody JS, *et al*. Angiosarcoma outcomes and prognostic factors: a 25-year single institution experience. *Am J Clin Oncol* 2014; **37:** 473–479.
6. Behjati S, Tarpey PS, Sheldon H, *et al*. Recurrent PTPRB and PLCG1 mutations in angiosarcoma. *Nat Genet* 2014; **46:** 376–379.
7. Murali R, Chandramohan R, Möller I, *et al*. Targeted massively parallel sequencing of angiosarcomas reveals frequent activation of the mitogen activated protein kinase pathway. *Oncotarget* 2015; **6:** 36041–36052.
8. Painter CA, Jain E, Tomson BN, *et al*. The Angiosarcoma Project: enabling genomic and clinical discoveries in a rare cancer through patient-partnered research. *Nat Med* 2020; **26:** 181–187.
9. Chan JY, Lim JQ, Yeong J, *et al*. Multiomic analysis and immunoprofiling reveal distinct subtypes of human angiosarcoma. *J Clin Invest* 2020; **130:** 5833–5846.
10. Espejo-Freire AP, Elliott A, Rosenberg A, *et al*. Genomic landscape of angiosarcoma: a targeted and immunotherapy biomarker analysis. *Cancers (Basel)* 2021; **13:** 4816.
11. Wong K, Ludwig L, Krijgsman O, *et al*. Comparison of the oncogenomic landscape of canine and feline hemangiosarcoma shows novel parallels with human angiosarcoma. *Dis Model Mech* 2021; **14:** dmm049044.
12. Mukai C, Choi E, Sams KL, *et al*. Chromatin run-on sequencing analysis finds that ECM remodeling plays an important role in canine hemangiosarcoma pathogenesis. *BMC Vet Res* 2020; **16:** 206.
13. Wang G, Wu M, Durham AC, *et al*. Molecular subtypes in canine hemangiosarcoma reveal similarities with human angiosarcoma. *PLoS One* 2020; **15:** e0229728.
14. Gorden BH, Kim JH, Sarver AL, *et al*. Identification of three molecular and functional subtypes in canine hemangiosarcoma through gene expression profiling and progenitor cell characterization. *Am J Pathol* 2014; **184:** 985–995.
15. Weidema ME, van de Geer E, Koelsche C, *et al*. DNA methylation profiling identifies distinct clusters in angiosarcomas. *Clin Cancer Res* 2020; **26:** 93–100.
16. Florou V, Rosenberg AE, Wieder E, *et al*. Angiosarcoma patients treated with immune checkpoint inhibitors: a case series of seven patients from a single institution. *J Immunother Cancer* 2019; **7:** 213.
17. Frith AE, Hirbe AC, Van Tine BA. Novel pathways and molecular targets for the treatment of sarcoma. *Curr Oncol Rep* 2013; **15:** 378–385.
18. Hanna JA, Drummond CJ, Garcia MR, *et al*. Biallelic Dicer1 loss mediated by aP2-Cre drives angiosarcoma. *Cancer Res* 2017; **77:** 6109–6118.
19. Drummond CJ, Hanna JA, Garcia MR, *et al*. Hedgehog pathway drives fusion-negative rhabdomyosarcoma initiated from non-myogenic endothelial progenitors. *Cancer Cell* 2018; **33:** 108–124.e5.
20. Tang W, Zeve D, Suh JM, *et al*. White fat progenitor cells reside in the adipose vasculature. *Science* 2008; **322:** 583–586.
21. Murchison EP, Partridge JF, Tam OH, *et al*. Characterization of Dicer-deficient murine embryonic stem cells. *Proc Natl Acad Sci U S A* 2005; **102:** 12135–12140.
22. Jackson EL, Willis N, Mercer K, *et al*. Analysis of lung tumor initiation and progression using conditional expression of oncogenic K-ras. *Genes Dev* 2001; **15:** 3243–3248.
23. Aguirre AJ, Bardeesy N, Sinha M, *et al*. Activated Kras and Ink4a/Arf deficiency cooperate to produce metastatic pancreatic ductal adenocarcinoma. *Genes Dev* 2003; **17:** 3112–3126.
24. Uhlmann EJ, Wong M, Baldwin RL, *et al*. Astrocyte-specific TSC1 conditional knockout mice exhibit abnormal neuronal organization and seizures. *Ann Neurol* 2002; **52:** 285–296.
25. Madisen L, Zwingman TA, Sunkin SM, *et al*. A robust and high-throughput Cre reporting and characterization system for the whole mouse brain. *Nat Neurosci* 2010; **13:** 133–140.
26. Hanna JA, Garcia MR, Go JC, *et al*. PAX7 is a required target for microRNA-206-induced differentiation of fusion-negative rhabdomyosarcoma. *Cell Death Dis* 2016; **7**: e2256.
27. Hanna JA, Garcia MR, Lardennois A, *et al*. PAX3-FOXO1 drives miR-486-5p and represses miR-221 contributing to pathogenesis of alveolar rhabdomyosarcoma. *Oncogene* 2018; **37:** 1991–2007.
28. Langdon CG, Gadek KE, Garcia MR, *et al*. Synthetic essentiality between PTEN and core dependency factor PAX7 dictates rhabdomyosarcoma identity. *Nat Commun* 2021; **12:** 5520.
29. Benjamini Y, Hochberg Y. Controlling the false discovery rate: a practical and powerful approach to multiple testing. *J R Stat Soc B Methodol* 1995; **57:** 289–300.
30. Kim JH, Megquier K, Thomas R, *et al*. Genomically complex human angiosarcoma and canine hemangiosarcoma establish convergent

angiogenic transcriptional programs driven by novel gene fusions. *Mol Cancer Res* 2021; **19:** 847–861.
31. Love MI, Huber W, Anders S. Moderated estimation of fold change and dispersion for RNA-seq data with DESeq2. *Genome Biol* 2014; **15:** 550.
32. Subramanian A, Tamayo P, Mootha VK, *et al*. Gene set enrichment analysis: a knowledge-based approach for interpreting genome-wide expression profiles. *Proc Natl Acad Sci U S A* 2005; **102:** 15545–15550.
33. Mootha VK, Lindgren CM, Eriksson KF, *et al*. PGC-1alpha-responsive genes involved in oxidative phosphorylation are coordinately downregulated in human diabetes. *Nat Genet* 2003; **34:** 267–273.
34. Huang da W, Sherman BT, Lempicki RA. Systematic and integrative analysis of large gene lists using DAVID bioinformatics resources. *Nat Protoc* 2009; **4:** 44–57.
35. Kanehisa M, Goto S. KEGG: Kyoto encyclopedia of genes and genomes. *Nucleic Acids Res* 2000; **28:** 27–30.
36. Lee KY, Russell SJ, Ussar S, *et al*. Lessons on conditional gene targeting in mouse adipose tissue. *Diabetes* 2013; **62:** 864–874.
37. Van Dyck F, Scroyen I, Declercq J, *et al*. aP2-Cre-mediated expression activation of an oncogenic PLAG1 transgene results in cavernous angiomatosis in mice. *Int J Oncol* 2008; **32:** 33–40.
38. Shaheen NL, Kataria E, Antony J, *et al*. Extracellular matrix composition modulates angiosarcoma cell attachment and proliferation. *Oncoscience* 2017; **4:** 178–188.
39. Megquier K, Turner-Maier J, Swofford R, *et al*. Comparative genomics reveals shared mutational landscape in canine hemangiosarcoma and human angiosarcoma. *Mol Cancer Res* 2019; **17:** 2410–2421.
40. Kumar MS, Pester RE, Chen CY, *et al*. Dicer1 functions as a haploinsufficient tumor suppressor. *Genes Dev* 2009; **23:** 2700–2704.
41. Lambertz I, Nittner D, Mestdagh P, *et al*. Monoallelic but not biallelic loss of Dicer1 promotes tumorigenesis in vivo. *Cell Death Differ* 2010; **17:** 633–641.
42. Hatley ME, Tang W, Garcia MR, *et al*. A mouse model of rhabdomyosarcoma originating from the adipocyte lineage. *Cancer Cell* 2012; **22:** 536–546.
43. Kommalapati A, Tella SH, Durkin M, *et al*. Histiocytic sarcoma: a population-based analysis of incidence, demographic disparities, and long-term outcomes. *Blood* 2018; **131:** 265–268.
44. Fu Y, Luo N, Lopes-Virella MF. Oxidized LDL induces the expression of ALBP/aP2 mRNA and protein in human THP-1 macrophages. *J Lipid Res* 2000; **41:** 2017–2023.
45. Zindy F, Nilsson LM, Nguyen L, *et al*. Hemangiosarcomas, medulloblastomas, and other tumors in Ink4c/p53-null mice. *Cancer Res* 2003; **63:** 5420–5427.
46. Wagner MJ, Lyons YA, Siedel JH, *et al*. Combined VEGFR and MAPK pathway inhibition in angiosarcoma. *Sci Rep* 2021; **11:** 9362.
47. Kwiatkowski DJ, Zhang H, Bandura JL, *et al*. A mouse model of TSC1 reveals sex-dependent lethality from liver hemangiomas, and up-regulation of p70S6 kinase activity in Tsc1 null cells. *Hum Mol Genet* 2002; **11:** 525–534.
48. Leech JD, Lammers SH, Goldman S, *et al*. A vascular model of Tsc1 deficiency accelerates renal tumor formation with accompanying hemangiosarcomas. *Mol Cancer Res* 2015; **13:** 548–555.
49. Sun S, Chen S, Liu F, *et al*. Constitutive activation of mTORC1 in endothelial cells leads to the development and progression of lymphangiosarcoma through VEGF autocrine signaling. *Cancer Cell* 2015; **28:** 758–772.
50. Onda H, Lueck A, Marks PW, *et al*. Tsc2(+/-) mice develop tumors in multiple sites that express gelsolin and are influenced by genetic background. *J Clin Invest* 1999; **104:** 687–695.
51. Ferrell RE, Kimak MA, Lawrence EC, *et al*. Candidate gene analysis in primary lymphedema. *Lymphat Res Biol* 2008; **6:** 69–76.
52. Aranguren XL, Beerens M, Coppiello G, *et al*. COUP-TFII orchestrates venous and lymphatic endothelial identity by homo- or heterodimerisation with PROX1. *J Cell Sci* 2013; **126:** 1164–1175.
53. Wu J, Xu Y, Mo D, *et al*. Kaposi's sarcoma-associated herpesvirus (KSHV) vIL-6 promotes cell proliferation and migration by upregulating DNMT1 via STAT3 activation. *PLoS One* 2014; **9:** e93478.
54. Pan H, Zhong XP, Lee S. Sustained activation of mTORC1 in macrophages increases AMPKα-dependent autophagy to maintain cellular homeostasis. *BMC Biochem* 2016; **17:** 14.
55. Wang C, Haas MA, Yang F, *et al*. Autophagic lipid metabolism sustains mTORC1 activity in TSC-deficient neural stem cells. *Nat Metab* 2019; **1:** 1127–1140.
56. Yang F, Sun S, Wang C, *et al*. Targeted therapy for mTORC1-driven tumours through HDAC inhibition by exploiting innate vulnerability of mTORC1 hyper-activation. *Br J Cancer* 2020; **122:** 1791–1802.
57. Mansfield SA, Williams RF, Iacobas I. Vascular tumors. *Semin Pediatr Surg* 2020; **29:** 150975.
58. Saha J, Kim JH, Amaya CN, *et al*. Propranolol sensitizes vascular sarcoma cells to doxorubicin by altering lysosomal drug sequestration and drug efflux. *Front Oncol* 2020; **10:** 614288.
59. Foulkes WD, Priest JR, Duchaine TF. DICER1: mutations, microRNAs and mechanisms. *Nat Rev Cancer* 2014; **14:** 662–672.
60. Kasinski AL, Slack FJ. Epigenetics and genetics. MicroRNAs en route to the clinic: progress in validating and targeting microRNAs for cancer therapy. *Nat Rev Cancer* 2011; **11:** 849–864.
61. Lin S, Gregory RI. MicroRNA biogenesis pathways in cancer. *Nat Rev Cancer* 2015; **15:** 321–333.
62. Melo SA, Ropero S, Moutinho C, *et al*. A TARBP2 mutation in human cancer impairs microRNA processing and DICER1 function. *Nat Genet* 2009; **41:** 365–370.
63. Lu J, Getz G, Miska EA, *et al*. MicroRNA expression profiles classify human cancers. *Nature* 2005; **435:** 834–838.
64. Hill DA, Ivanovich J, Priest JR, *et al*. DICER1 mutations in familial pleuropulmonary blastoma. *Science* 2009; **325:** 965.
65. Chen S, Xue Y, Wu X, *et al*. Global microRNA depletion suppresses tumor angiogenesis. *Genes Dev* 2014; **28:** 1054–1067.
66. Ravi A, Gurtan AM, Kumar MS, *et al*. Proliferation and tumorigenesis of a murine sarcoma cell line in the absence of DICER1. *Cancer Cell* 2012; **21:** 848–855.
67. Thibodeau BJ, Lavergne V, Dekhne N, *et al*. Mutational landscape of radiation-associated angiosarcoma of the breast. *Oncotarget* 2018; **9:** 10042–10053.
68. Liang X, Gupta K, Quintero JR, *et al*. Macrophage FABP4 is required for neutrophil recruitment and bacterial clearance in Pseudomonas aeruginosa pneumonia. *FASEB J* 2019; **33:** 3562–3574.
69. Carrasco DR, Fenton T, Sukhdeo K, *et al*. The PTEN and INK4A/ARF tumor suppressors maintain myelolymphoid homeostasis and cooperate to constrain histiocytic sarcoma development in humans. *Cancer Cell* 2006; **9:** 379–390.
70. Shanmugam V, Griffin GK, Jacobsen ED, *et al*. Identification of diverse activating mutations of the RAS-MAPK pathway in histiocytic sarcoma. *Mod Pathol* 2019; **32:** 830–843.
71. Egan C, Nicolae A, Lack J, *et al*. Genomic profiling of primary histiocytic sarcoma reveals two molecular subgroups. *Haematologica* 2020; **105:** 951–960.
72. Chadwick ML, Lane A, Thomas D, *et al*. Combined mTOR and MEK inhibition is an effective therapy in a novel mouse model for angiosarcoma. *Oncotarget* 2018; **9:** 24750–24765.
73. Du W, Gerald D, Perruzzi CA, *et al*. Vascular tumors have increased p70 S6-kinase activation and are inhibited by topical rapamycin. *Lab Invest* 2013; **93:** 1115–1127.

74. Yoo C, Lee J, Rha SY, *et al*. Multicenter phase II study of everolimus in patients with metastatic or recurrent bone and soft-tissue sarcomas after failure of anthracycline and ifosfamide. *Invest New Drugs* 2013; **31:** 1602–1608.
75. Zukerberg LR, Nickoloff BJ, Weiss SW. Kaposiform hemangioendothelioma of infancy and childhood. An aggressive neoplasm associated with Kasabach-Merritt syndrome and lymphangiomatosis. *Am J Surg Pathol* 1993; **17:** 321–328.
76. Wang Z, Yao W, Sun H, *et al*. Sirolimus therapy for kaposiform hemangioendothelioma with long-term follow-up. *J Dermatol* 2019; **46:** 956–961.
77. Hammill AM, Wentzel M, Gupta A, *et al*. Sirolimus for the treatment of complicated vascular anomalies in children. *Pediatr Blood Cancer* 2011; **57:** 1018–1024.
78. Salter DM, Griffin M, Muir M, *et al*. Development of mouse models of angiosarcoma driven by p53. *Dis Model Mech* 2019; **12:** dmm038612.

SUPPLEMENTARY MATERIAL ONLINE

Supplementary materials and methods

Figure S1. Signaling pathways in AD^{cKO} and AKC^{cKO} angiosarcoma mouse models

Figure S2. *Dicer1* loss and *Kras* activation or *Cdkn2a* deletion cooperate to drive angiosarcoma development

Figure S3. Validation of ADC106 murine angiosarcoma cell line

Figure S4. Angiosarcomas in $AD^{cKO}T^{cKO}$ mice

Figure S5. AT^{cKO} tumors resemble KHE-like tumors

Figure S6. Gene expression alterations in vascular mouse tumors

Table S1. Mouse strains used in this study

Table S2. Antibodies used for immunoblots

Table S3. Antibodies used for IHC

Table S4. KEGG pathways enriched in AD^{cKO} and AKC^{cKO} murine angiosarcomas

Table S5. Gene ontology analysis of AT^{cKO} tumors

Table S6. RPPA analysis of AT^{cKO} tumors

Table S7. Summary of GEMMs and associated phenotypes

Table S8. Primers for RT-qPCR